HIGH-EFFICIENCY AMORPHOUS SILICON AND NANOCRYSTALLINE SILICON BASED SOLAR CELLS AND MODULES

Quarterly Technical Progress Report
February 1 through April 30, 2006

S. Guha and J. Yang
United Solar Ovonic Corporation
Troy, Michigan

NREL Technical Monitor: Bolko von Roedern

Prepared under Subcontract No. ZXL-6-44205-14

Preface

The previous Thin Film Partnership Subcontract No. ZDJ-2-30630-19 ended on May 31, 2005. The new Subcontract No. ZXL-6-44205-14 started on February 1, 2006. Therefore, this quarterly Subcontract Report partially covers the work performed by United Solar Ovonic Corporation for the period from June 1, 2005 to April 30, 2006 even though the financial support started from February 1, 2006. The following personnel participated in this research program.

A. Banerjee, E. Chen, G. Fischer, G. Ganguly, S. Guha (Principal Investigator), B. Hang, M. Hopson, A. Mohsin, J. Noch, J. M. Owens, T. Palmer, D. Wolf, B. Yan, J. Yang (Co-Principal Investigator), K. Younan, and G. Yue.

Collaboration with the Colorado School of Mines, University of Oregon, Syracuse University, and National Renewable Energy Laboratory is acknowledged. We would like to thank S. R. Ovshinsky and H. Fritzsche for their constant encouragement and useful discussion.

Executive Summary

Objectives

United Solar Ovonic Corporation (United Solar) has successfully used its spectrum splitting, a-Si:H/a-SiGe:H/a-SiGe:H triple-junction structure in the 25 MW manufacturing plant, and will use the same technology in its next 25 MW plant, which will start production by the end of 2006. In order to improve the solar panel efficiency and reduce the manufacturing cost, we need to explore new materials, new cell structures, and new deposition processes. Under support from the previous Thin Film Partnership Program, United Solar has studied the possibility of using hydrogenated nanocrystalline silicon (nc-Si:H) for possible substituting amorphous silicon germanium alloy (a-SiGe:H) in the bottom cell of the triple-junction structure. The main objective of the current project is to continue investigating issues related to nc-Si:H material properties, cell efficiency, and deposition rate. The major target is to demonstrate the feasibility of using nc-Si:H in multi-junction structures and achieve higher cell and module efficiencies than those achieved using the conventional a-Si:H/a-SiGe:H/a-SiGe:H triple-junction configuration.

Approaches

We continue to optimize the hydrogen dilution profiling for controlling the evolution of nc-Si:H. At the same time, we re-modified the VHF deposition chamber to make it suitable for high pressure deposition. In addition, we optimized the a-Si:H top cell and a-SiGe:H middle cell for high efficiency triple-junction structure. With collaboration from NREL, we also investigated the mechanism of light-induced degradation in the nc-Si:H solar cells and explored ways to reduce the magnitude of light-induced degradation in nc-Si:H.

Status/Accomplishments

1. We have achieved active-area (0.25 cm^2) initial and stable efficiencies of 9.0% and 8.5%, respectively, for nc-Si:H single-junction cells made with MVHF at a high rate ~ 5-8 Å/s.
2. We have achieved active-area (0.25 cm^2) initial and stable efficiencies of 15.1% and 13.3%, respectively, for an a-Si:H/a-SiGe:H/nc-Si:H triple-junction cell, where the top and middle cells were made using RF at a low rate ~ 1 Å/s, and the nc-Si:H bottom cell using MVHF at a high rate ~ 5-8 Å/s.
3. We have achieved active-area (0.25 cm^2) initial and stable efficiencies of 14.1% and 13.3%, respectively, for an a-Si:H/nc-Si:H/nc-Si:H triple-junction cell, where the top cell was made using RF at a low rate ~ 1 Å/s, and the nc-Si:H middle and bottom cells using MVHF at a high rate ~ 5-8 Å/s.
4. We have demonstrated that an optimized hydrogen dilution profiling not only improves the initial nc-Si:H cell performance but also improves the stability against light soaking.
5. We have shown that the light-induced degradation can be reduced to as low as 3-5% for a-Si:H/nc-Si:H/nc-Si:H triple-junction solar cells by improving the nc-Si:H cell stability.

1. High Efficiency Hydrogenated Amorphous Silicon Based Triple-Junction Solar Cells Incorporating Nanocrystalline Silicon

1.1. INTRODUCTION

A world record stable cell efficiency of 13.0% was achieved previously by using hydrogenated amorphous silicon (a-Si:H) and silicon germanium (a-SiGe:H) alloys in a spectrum-splitting, triple-junction structure [1]. This technology has been used in United Solar's 25 MW production line [2] and will be used in the next 25 MW plant. In recent years, hydrogenated nanocrystalline silicon (nc-Si:H) has attracted remarkable attention due to its superior long wavelength response and reported improved stability. Significant progress has been made resulting in cell efficiency approaching 15% [3] and module efficiency of over 13% [4]. In our laboratory, we have focused on the development of nc-Si:H solar cells and explored the possibility of substituting nc-Si:H for the a-SiGe:H middle and bottom cells in our triple-junction structure. We have carried out various studies for improving the nc-Si:H cell performance, stability, and deposition rate [5-8]. A hydrogen dilution profiling technique has been developed and shown to be an effective way of controlling the nc-Si:H material structure and improving the cell performance [7]. Using this technique, we have recently reported an initial active-area efficiency of 14.6% for an a-Si:H/a-SiGe:H/nc-Si:H triple-junction structure [8]. In the past year, we have focused on the optimization of nc-Si:H solar cells at high rates and used the optimized nc-Si:H cell in a-Si:H/a-SiGe:H/nc-Si:H and a-Si:H/nc-Si:H/nc-Si:H triple-junction structures. We have made considerable progress in the improvement of cell efficiency.

1.2. EXPERIMENTAL

Single-junction *n-i-p* a-Si:H top and a-SiGe:H middle cells were deposited on bare stainless steel (SS) substrate using RF glow discharge. nc-Si:H single-junction bottom cells and triple-junction structures were fabricated on Ag/ZnO back reflector coated SS substrate with the intrinsic nc-Si:H layer deposited using modified very high frequency (MVHF) glow discharge at high rates ~5-8 Å/s. We have modified our deposition system based on the requirements of newly developed deposition parameters. The deposition parameters, such as pressure, substrate temperature, hydrogen dilution, and VHF power, have been re-optimized. Indium-Tin-Oxide dots with an active-area of 0.25 cm^2 were deposited on top of the *p* layer as the top transparent contact. Current density versus voltage (J-V) characteristics were measured under an AM1.5 solar simulator. The middle and bottom cells were also measured with long-pass filters. Quantum efficiency (QE) was measured for a wavelength range of 300 to 1100 nm. Light-soaking experiments were carried out with ~100 mW/cm^2 white light at 50 ºC.

1.3. RESULTS AND DISCUSSION

1.3.1. Optimization of a-SiGe:H middle cells

For high efficiency multi-junction solar cells, each component cell as well as the tunnel junction between the component cells have to be optimized. It is now well known that hydrogen dilution is an effective way for improving the a-Si:H and a-SiGe:H cell performance. In this study, we have systematically optimized the a-Si:H top and a-SiGe:H middle cells with hydrogen dilution approaching the amorphous to nanocrystalline transition. Compared to the conventional a-Si:H/a-

SiGe:H/a-SiGe:H triple-junction structure, the a-Si:H top and a-SiGe:H middle cells need to have higher current densities in an a-Si:H/a-SiGe:H/nc-Si:H triple-junction structure for the following two reasons. First, the nc-Si:H bottom cell has a higher short-circuit current density (J_{sc}), but lower open-circuit voltage (V_{oc}). Second, a current mismatch having the current limited by the nc-Si:H bottom cell results in a higher fill factor (FF). The challenge is to obtain an a-SiGe:H middle cell with a high current density. Normally, increasing the intrinsic layer thickness and/or the Ge content can increase the J_{sc}. However, both methods may cause a reduction in V_{oc} and FF. In order to obtain an a-SiGe:H middle cell having a high J_{sc}, we have re-optimized the hydrogen dilution rate and other parameters, such as the pressure and substrate temperature. We tried to keep the material structure close to the amorphous to nanocrystalline transition. Table I lists the J-V characteristics of a-SiGe:H middle cells made with various hydrogen dilutions, where the J-V was measured under an AM1.5 solar simulator with a 530-nm long pass filter, and using the integrated QE value for the J_{sc}. One can see that an optimized hydrogen dilution increases the maximum power (P_{max}), mainly due to the improved FF. Increasing the a-SiGe:H intrinsic layer thickness increases the J_{sc}, but slightly reduces V_{oc} and FF. The overall P_{max} is still improved.

Table I: J-V characteristics of a-SiGe:H middle cells on SS substrate, where B denotes baseline, OH optimized hydrogen dilution, TI thicker intrinsic layer, and OD over dilution. The measurement was made under an AM1.5 solar simulator with a 530-nm long pass filter.

Sample	J_{sc} (mA/cm^2)	V_{oc} (V)	FF	P_{max} (mW/cm^2)	Comment
15318	9.26	0.757	0.708	4.96	B
15326	9.55	0.754	0.716	5.16	OH
15329	10.47	0.747	0.686	5.37	OH+TI
15333	10.47	0.744	0.693	5.40	OH+TI
15334	9.82	0.651	0.660	4.22	OD

1.3.2. Optimization of MVHF nc-Si:H cell at high rates

The major contribution to the high efficiency triple-junction cell is the improved nc-Si:H bottom cell. Two important techniques were used for the optimization of the nc-Si:H material quality. First, a proper hydrogen dilution profiling was used to control the evolution of nanocrystallites along the growth direction. We found that the hydrogen dilution profiling improves not only the nc-Si:H cell performance [7,8], but also the stability [9]. Second, the nc-Si:H intrinsic layer was deposited in a high pressure and high power regime [10,11]. Under this condition, the quality of the high rate deposited nc-Si:H material is improved. Table II lists the J-V characteristics of nc-Si:H single-junction solar cells suitable for use in the middle and the bottom cells. An initial active-area cell efficiency of 8.99% has been achieved. Figure 1 shows the J-V characteristics and QE of the best nc-Si:H single-junction cell. This cell shows a large V_{oc} but a moderate J_{sc}, which is suitable for the middle cell in triple-junction structures. We light soaked the high efficiency nc-Si:H cell under 100 mW/cm^2 white light at 50 °C for over 1000 hours and obtained a stabilized efficiency of 8.5%. The 5.5% light-induced degradation is mainly due to a reduction in the J_{sc}. The QE curve reveals a reduction in the short wavelength region, which does not affect its performance in a multi-junction structure [9]. We have also developed nc-Si:H single-junction cells with high long wavelength response for the bottom cell in triple-junction structures. Figure 2 shows the J-V

Table II: Initial active-area performance of nc-Si:H solar cells made with MVHF at high rates.

Sample	Eff (%)	J_{sc} (mA/cm^2)	V_{oc} (V)	FF	Comment
13831	8.99	23.59	0.568	0.671	middle
13821	8.65	24.44	0.552	0.641	
13829	8.48	23.11	0.566	0.648	
13935	8.81	26.94	0.538	0.608	bottom
14173	7.78	26.65	0.500	0.584	
14191	7.86	26.36	0.478	0.624	

characteristics and QE of the best nc-Si:H cell used as the bottom cell in a triple-junction structure. The total current density is ~27 mA/cm^2 with long wavelength response extending to 1100 nm.

1.3.3. High efficiency triple-junction solar cells

We used the optimized component cells to fabricate triple-junction cells. Table III lists the J-V characteristics of several a-Si:H/a-SiGe:H/nc-Si:H cells in the initial and light-soaked states, where the light-soaked state was reached by light soaking under ~100 mW/cm^2 white light at 50 ºC for 575 hours. The highest initial active-area efficiency of 15.1% is achieved using this triple-junction structure. The initial J-V characteristics and QE are shown in Fig. 3. After light soaking, a stable efficiency of 13.3% is obtained. From the data in Table III, one can see that the bottom cell current did not degrade after light soaking; having the bottom cell limited current mismatching resulted in the lowest degradation. The light induced degradation is only 6.7%. However, the cell with the highest initial efficiency degraded by 17.1%, mainly due to a large reduction of FF caused by the middle cell limited current mismatching.

Table III: J-V characteristics of high efficiency a-Si:H/a-SiGe:H/nc-Si:H triple-junction solar cells. Deg. denotes the percentage of light-induced degradation. The bold numbers are the highest efficiencies and italic numbers are the limited current densities for J_{sc}.

Sample	State	Eff (%)	J_{sc} (mA/cm^2)	QE (mA/cm^2)			V_{oc} (V)	FF
				top	middle	bottom		
15501-34	Initial	14.77	9.11	*9.11*	9.24	9.20	2.145	0.756
	Stable	12.62	8.69	8.85	*8.69*	9.12	2.101	0.691
	Deg.	14.6%	4.6%	2.9%	6.0%	0.9%	2.1%	8.6%
15506-33	Initial	**15.07**	9.13	*9.13*	9.27	9.31	2.195	0.752
	Stable	12.49	8.63	8.74	*8.63*	9.24	2.116	0.684
	Deg.	17.1%	5.5%	4.3%	6.9%	0.8%	3.6%	9.0%
15506-34	Initial	14.27	8.72	9.25	9.41	*8.72*	2.167	0.755
	Stable	**13.31**	8.72	8.90	8.76	*8.72*	2.132	0.716
	Deg.	6.7%	0	3.8%	6.9%	0	1.6%	5.2%

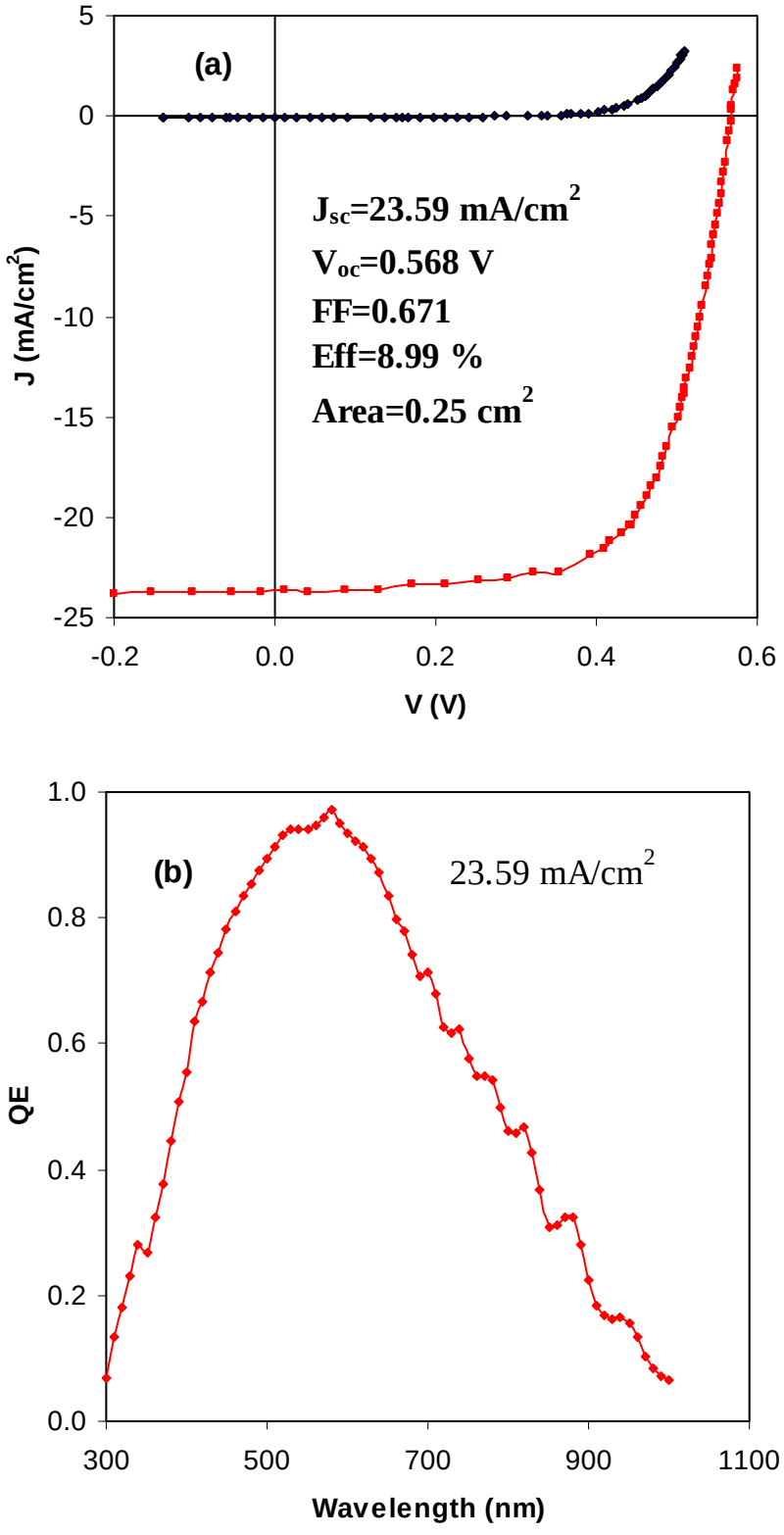

Figure 1. (a) J-V characteristics and (b) quantum efficiency of a nc-Si:H solar cell as the middle cell in a triple-junction structure.

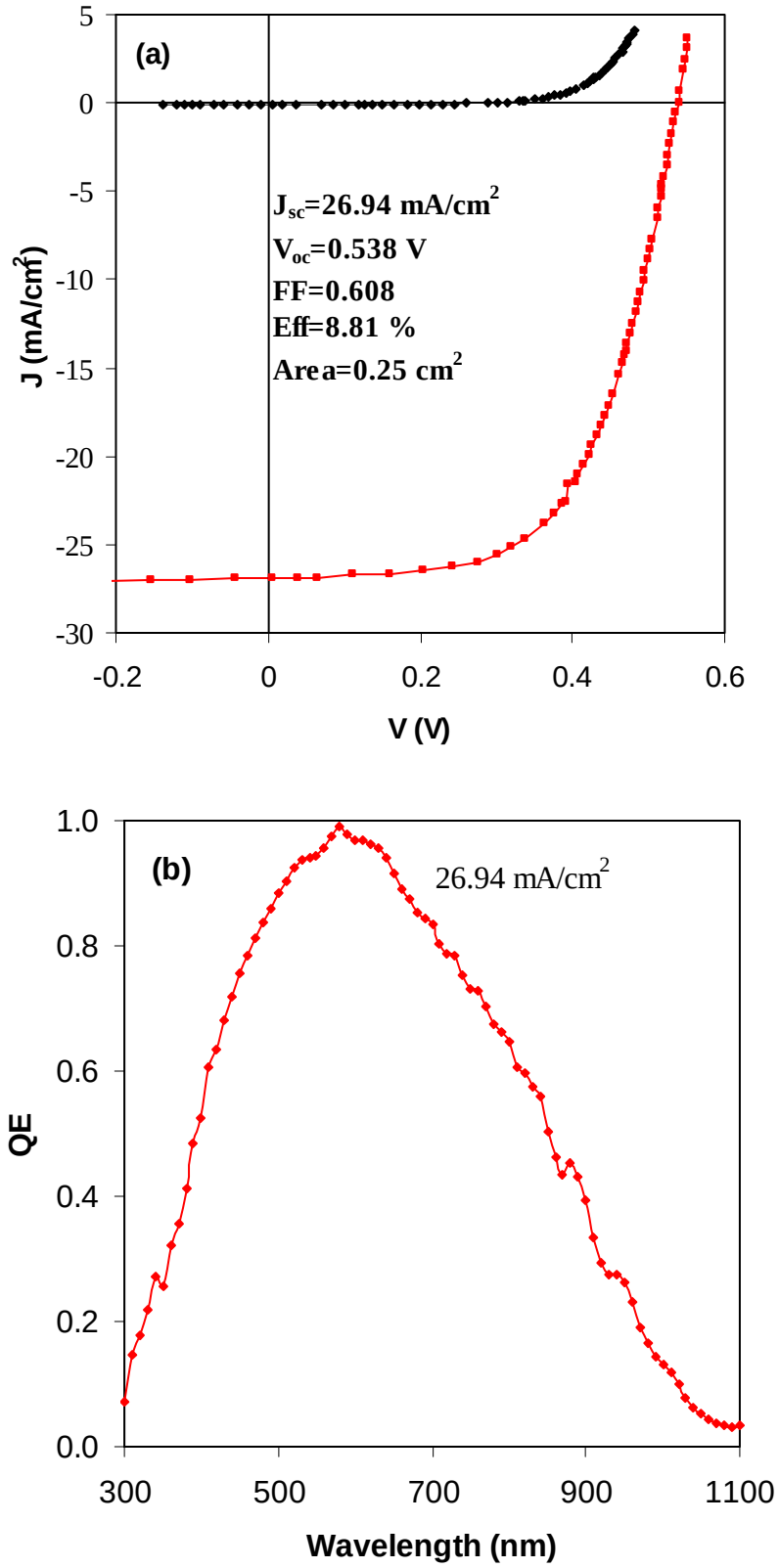

Figure 2. (a) J-V characteristics and (b) quantum efficiency of a nc-Si:H solar cell as the bottom cell in a triple-junction structure.

Table IV: J-V characteristics of high efficiency a-Si:H/nc-Si:H/nc-Si:H triple-junction solar cells. Deg. denotes the percentage of light-induced degradation. The bold numbers are the highest efficiencies and italic numbers are the limited current densities for $J_{sc.}$

Sample	State	Eff (%)	J_{sc} (mA/cm^2)	QE (mA/cm^2)			V_{oc} (V)	FF
				top	middle	bottom		
13955-33	Initial	**14.14**	9.11	9.11	9.72	*9.11*	1.965	0.790
	Stable	13.19	8.79	*8.79*	9.56	9.04	1.947	0.771
	Deg.	6.7%	3.5%	3.5%	1.6%	0.8%	0.9%	2.4%
13955-24	Initial	13.86	8.89	9.02	9.52	*8.89*	1.981	0.787
	Stable	**13.26**	8.72	8.75	9.25	*8.72*	1.973	0.771
	Deg.	4.3%	1.9%	3.0%	2.8%	1.9%	0.4%	2.0%
14005-33	Initial	13.67	8.99	9.44	9.54	*8.99*	1.944	0.782
	Stable	13.24	8.92	9.04	9.42	*8.92*	1.933	0.768
	Deg.	3.1%	0.8%	4.2%	1.3%	0.8%	0.6%	1.8%

Table IV summarizes the J-V characteristics of several a-Si:H/nc-Si:H/nc-Si:H triple-junction solar cells in the initial and light-soaked states, where the light-soaked state was reached by light soaking under ~100 mW/cm^2 white light at 50 ºC for over 1000 hours. The highest initial active-area efficiency of 14.1% is achieved with the initial J-V characteristics and QE shown in Fig. 4. Although the a-Si:H/nc-Si:H/nc-Si:H triple-junction structure does not yield the highest initial efficiency, it shows a very small light-induced degradation of 4.3%, resulting from a better stability of the nc-Si:H middle cell compared to the a-SiGe:H middle cell. A stable active-area efficiency of 13.3% is also achieved with this cell structure.

1.4. SUMMARY

We have made significant progress in the optimization of a-Si:H, a-SiGe:H, and nc-Si:H materials and devices for high efficiency triple-junction solar cells. The a-Si:H top and a-SiGe:H middle cells have been re-optimized for matching the high current from the nc-Si:H bottom cell. The nc-Si:H bottom cell has been improved using MVHF in the high pressure regime. An optimized hydrogen dilution profiling is the key technique for optimizing the growth of the nc-Si:H material, which is a critical element for obtaining high efficiency nc-Si:H solar cells. Based on these techniques, we have achieved initial and stable active-area efficiencies of 15.1% and 13.3%, respectively, using the a-Si:H/a-SiGe:H/nc-Si:H triple-junction structure. The stability of triple-junction cells is improved by substituting the a-SiGe:H middle cell by nc-Si:H. Using the a-Si:H/nc-Si:H/nc-Si:H triple-junction structure, we have obtained an initial active-area efficiency of 14.1%. After prolonged light soaking, the a-Si:H/nc-Si:H/nc-Si:H triple-junction cell also stabilized at 13.3%. The stable triple-junction cell efficiency incorporating nc-Si:H material is higher than the previous record of 13.0% achieved using the conventional a-Si:H/a-SiGe:H/a-SiGe:H triple-junction structure [1]. Figure 5 plots the progress made in the efficiency of triple-junction solar cells incorporating nc-Si:H. One can see that a significant progress has been made and further improvements can be expected in the near future.

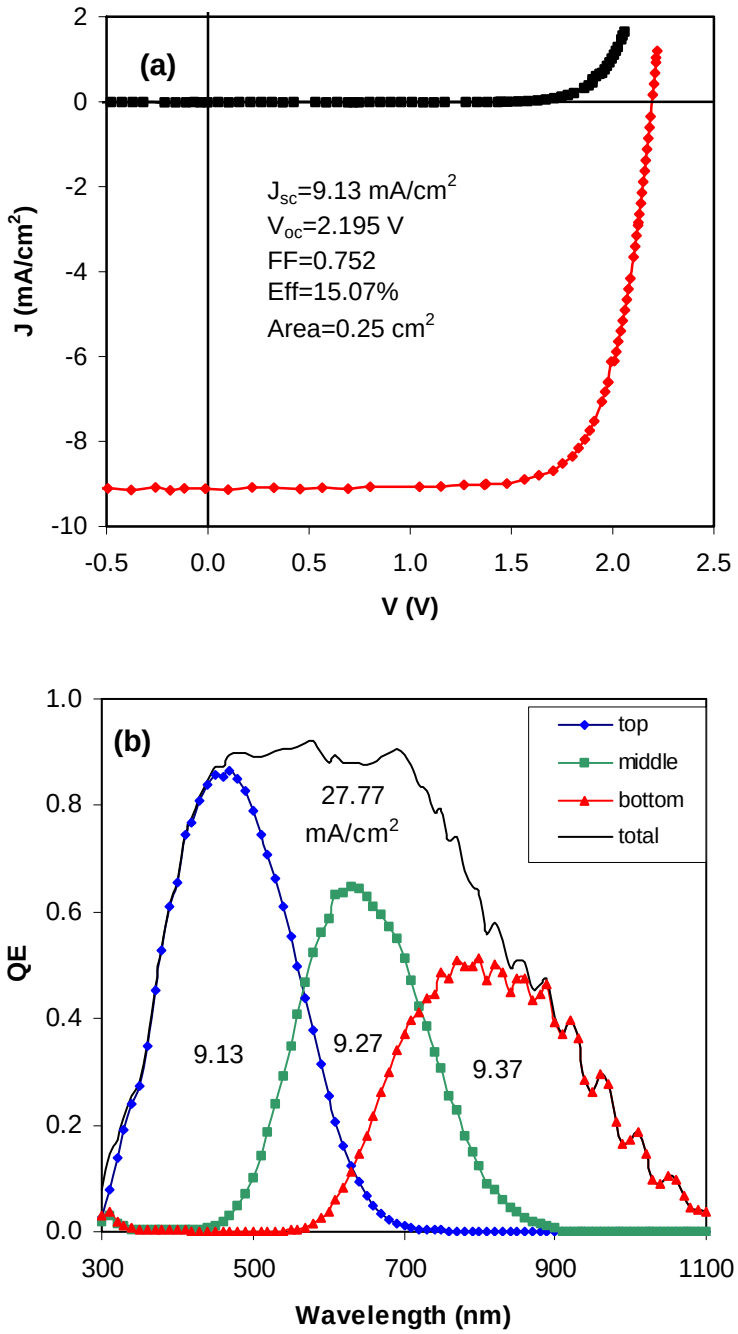

Figure 3. (a) J-V characteristics and (b) quantum efficiency of an a-Si:H/a-SiGe:H/nc-Si:H triple-junction solar cell.

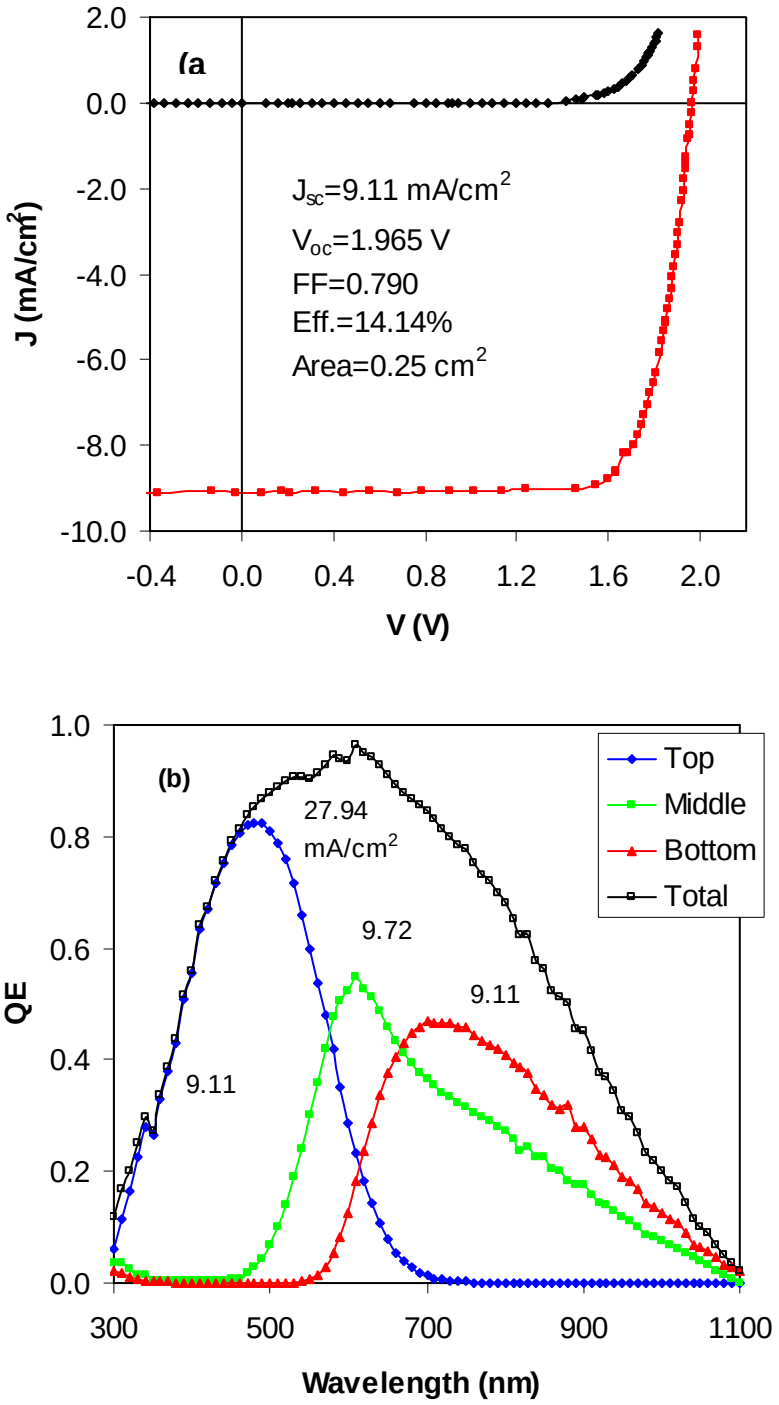

Figure 4. (a) J-V characteristics and (b) quantum efficiency of an a-Si:H/nc-Si:H/nc-Si:H triple-junction solar cell.

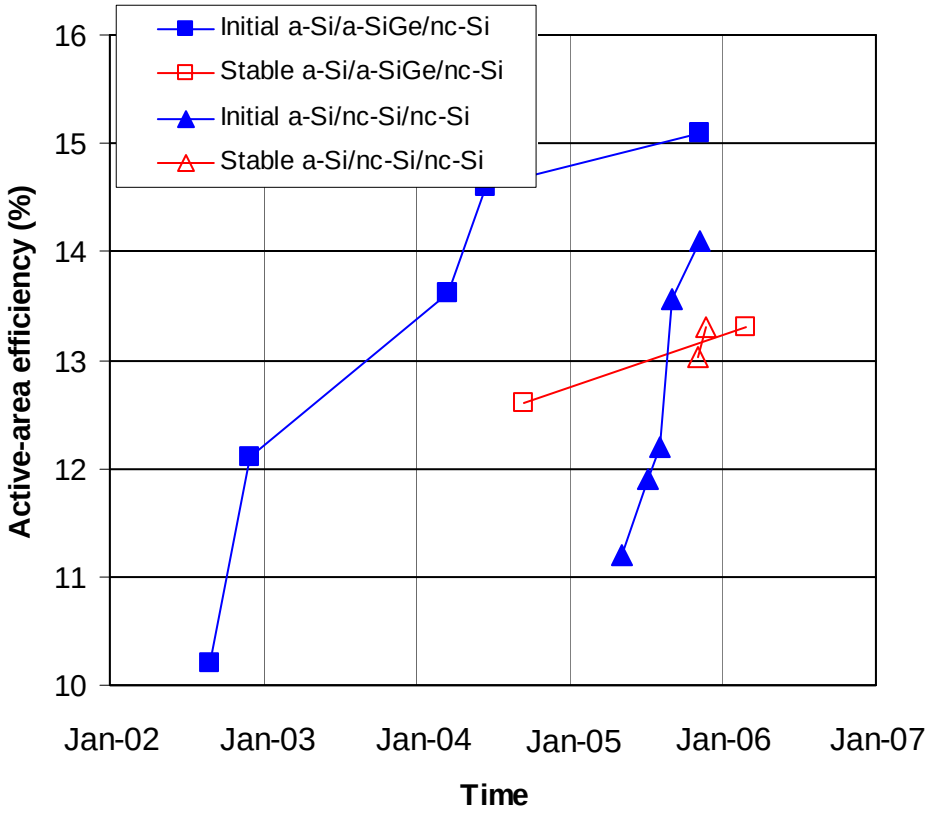

Figure 5. Progress made in a-Si:H/a-SiGe:H/nc-Si:H and a-Si:H/nc-Si:H/nc-Si:H triple-junction solar cells at United Solar Ovonic Corporation.

2. Material Structure and Metastability of Hydrogenated Nanocrystalline Silicon Solar Cells

2.1. INTRODUCTION

nc-Si:H has attracted significant attention as a narrow band gap intrinsic layer in multi-junction solar cells for its superior long wavelength response and stability. Previously, several groups reported that there was no light-induced degradation in nc-Si:H solar cells [12-14]. However, we found that nc-Si:H single-junction cells made in our laboratory showed light-induced degradations in the range of 3% to 15% [15-17]. In addition, the light-induced degradation was surprisingly increased by applying a reverse electrical bias during light soaking [16,17], contrary to the decreased degradation observed in a-Si:H solar cells. We proposed a back-to-back micro-diode model to explain the enhanced light-induced degradation by a reverse bias in the nc-Si:H solar cells [16,17]. A wavelength dependent light-soaking study showed that the light-induced degradation mainly occurs in the amorphous and/or grain boundary regions [15]. Meanwhile, several recent reports showed that the light-induced degradation is dominated by the amount of amorphous component in the nc-Si:H intrinsic layer [18,19]. On the other hand, nc-Si:H cells made near the nanocrystalline/amorphous transition that usually have a large volume fraction of amorphous component show the best performance [20]. In order to improve the nc-Si:H cell performance and stability at the same time, a better understanding of the factors determining the metastability is essential.

We have made significant progress in understanding the mechanism of light-induced degradation in nc-Si:H solar cells [15-17]. We have also tried to improve the stability of the nc-Si:H cell by optimizing the deposition process and device design. As previously reported, hydrogen dilution profiling is an effective method of controlling the nanocrystalline evolution during the deposition of nc-Si:H, and improves the initial solar cell performance [10].

In this quarter, we have systematically studied the metastability of nc-Si:H solar cells made with various hydrogen dilution profiles and correlate the results to the material structural properties. Using the gathered knowledge, we have further optimized the material structure and improved the cell performance and stability. As a result, we have achieved initial and stable active-area efficiencies of 14.1% and 13.3%, respectively, using an a-Si:H/nc-Si:H/nc-Si:H triple-junction structure, as presented in the previous section.

2.2. EXPERIMENTAL

Most of the nc-Si:H single-junction and a-Si:H/nc-Si:H/nc-Si:H triple-junction solar cells reported here were deposited using a multi-chamber glow discharge system with RF excitation for the doped layers and a modified VHF (MVHF) technique for the intrinsic nc-Si:H layers. Some of the cells have an RF deposited nc-Si:H film as the intrinsic layer. The nanostructure evolution in the nc-Si:H intrinsic layer was controlled by hydrogen dilution profiling with decreasing dilution ratio during the deposition. The profiling was achieved both by continuously changing the dilution (dynamic profiling) and by changing dilution in three discrete steps during deposition (step profiling). Light soaking was carried out with a 100 mW/cm^2 white light at 50 °C under the open circuit condition for over 1000 hours. The current-density versus voltage (J-V) characteristics were measured under an AM1.5 solar simulator at 25 °C. Quantum efficiency (QE) was measured from 300 nm to 1100 nm. The material structure of the intrinsic layer was directly measured on the solar cells using Raman spectroscopy with different excitation wavelengths.

2.3. RESULTS AND DISCUSSION

Table V lists the J-V characteristics of two sets of nc-Si:H single-junction solar cells at their initial and stable states. The intrinsic nc-Si:H layers in the first set (the first three cells) were deposited using RF. MVHF was used for the nc-Si:H intrinsic layer deposition in the second set (the last three cells). The first two RF cells using a constant hydrogen dilution during the intrinsic layer deposition show a large light-induced degradation of 14-15% in efficiency, mainly due to reductions in open-circuit voltage (V_{oc}) and fill factor (FF). The third cell, with an optimized hydrogen dilution profiling, shows only a 3.5% light-induced degradation. Similarly, for the MVHF cells, the cell with a step hydrogen dilution profiling shows an 8.5% light-induced degradation, which is somewhat lower than the RF cells with constant hydrogen dilution, but is still much larger than the two dynamically profiled cells. The V_{oc} and FF in the MVHF cell (13348) with an optimized hydrogen dilution profiling did not degrade after prolonged light soaking; in fact, the FF of this cell was slightly improved.

In order to obtain a better understanding of the mechanism of the light-induced degradation of nc-Si:H solar cells and its relation to the deposition process as well as material structures, Raman measurements were carried out directly on the six solar cells. Figure 6 shows the Raman spectra of the sample 10521 excited with a green (532 nm) laser and a red (633 nm) laser. The green light probes the material structure in the top layer near the *i/p* interface, while the red light reveals the information from the bulk of the intrinsic layer. One can see that the crystalline volume fraction is higher in the top layer (measured with the green laser) near the *i/p* interface than in the bulk. This result is consistent

Table V: Initial (A) and stable (B) performance of nc-Si:H cells. C refers to the percentage of light-induced change.

Run #	Dep. Method	H Dilution	State	Eff (%)	J_{sc} (mA/cm^2)	V_{oc} (V)	FF
10514	RF	Constant	A	7.85	23.06	0.499	0.682
			B	6.73	22.44	0.470	0.638
			C	-14.3%	-2.7%	-5.8%	-6.5%
10521	RF	Constant	A	7.21	23.03	0.461	0.679
			B	6.12	22.65	0.426	0.634
			C	-15.1%	-1.7%	-7.6%	-6.6%
10505	RF	Dynamic Profiling	A	7.56	22.76	0.520	0.638
			B	7.30	22.91	0.517	0.616
			C	-3.5%	+0.7%	-0.6%	-3.4%
12085	MVHF	Step Profiling	A	6.62	21.76	0.479	0.635
			B	6.06	21.65	0.470	0.596
			C	-8.5%	-0.5%	-1.9%	-6.1%
13324	MVHF	Dynamic Profiling	A	6.75	23.89	0.490	0.577
			B	6.52	23.16	0.481	0.585
			C	-3.4%	-3.1%	-1.8%	+1.4%
13348	MVHF	Dynamic Profiling	A	7.82	22.72	0.524	0.657
			B	7.72	21.85	0.527	0.670
			C	-1.3%	-3.9%	+0.6%	+2.0%

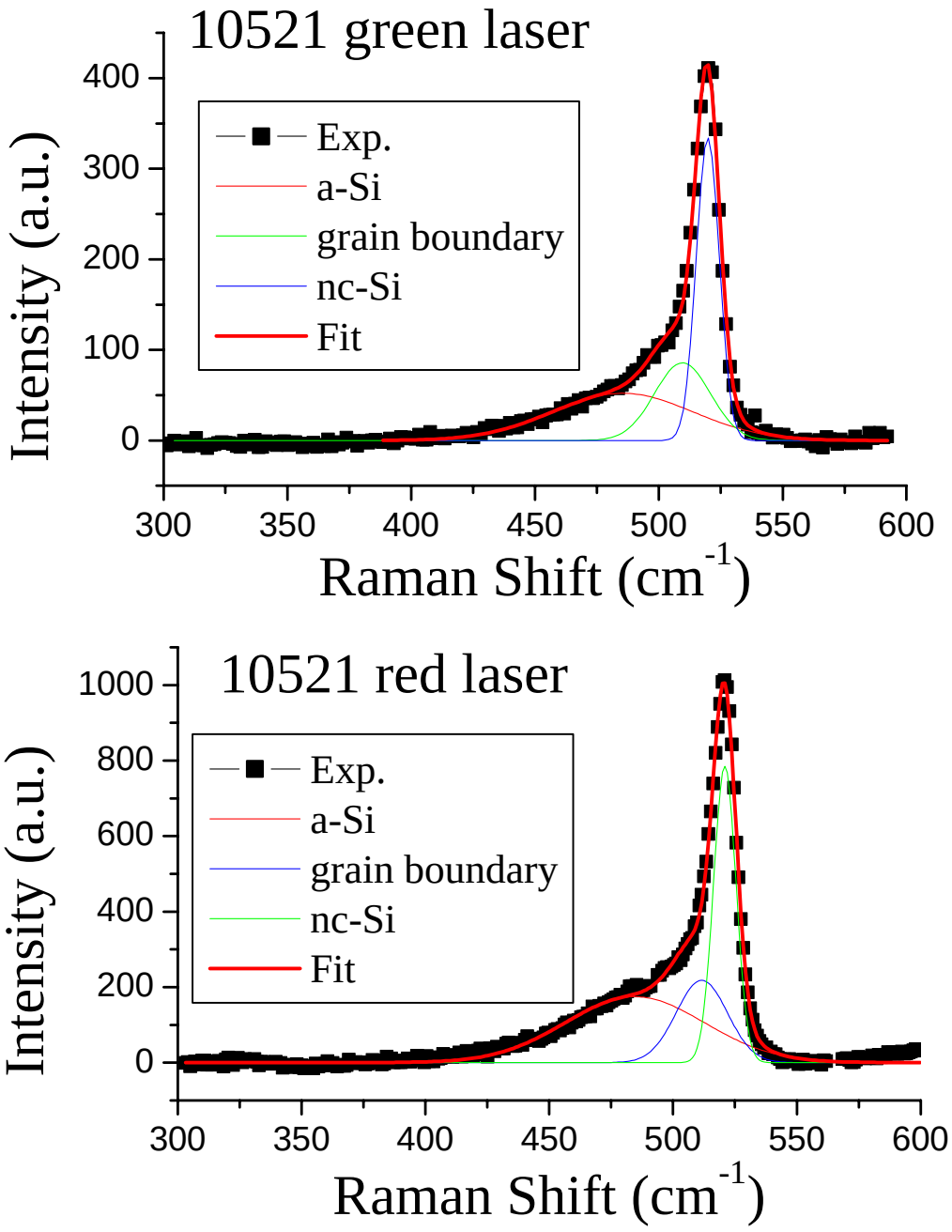

Figure 6. Raman spectra and their deconvolutions of cell 10521 excited with (upper) a green laser and (lower) a red laser.

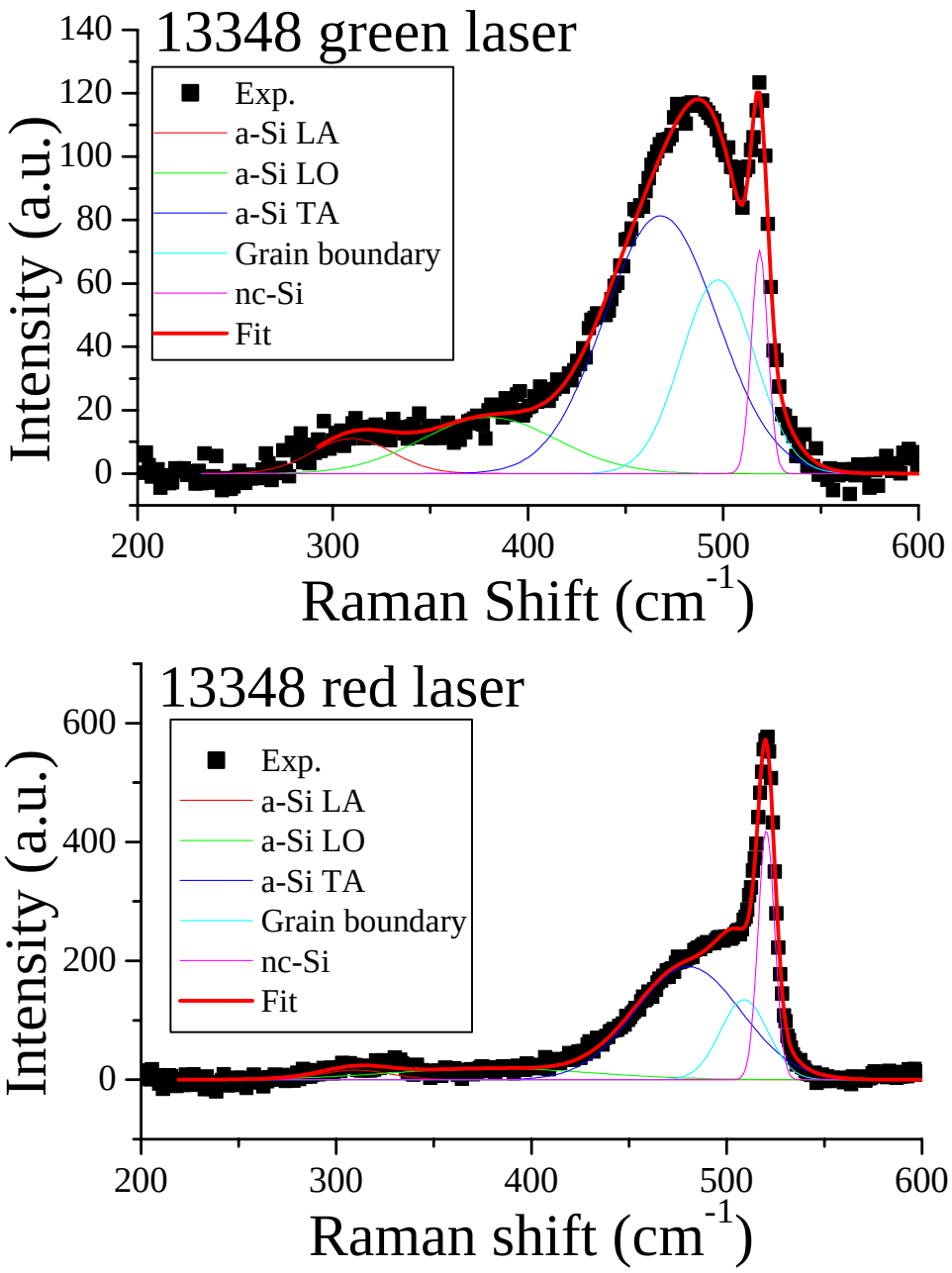

Figure 7. Raman spectra and their deconvolutions of cell 13348 excited with (upper) a green laser and (lower) a red laser.

with the normally observed nanocrystalline evolution with thickness. Figure 7 shows the Raman spectra of the sample 13348 (made with MVHF) excited with a green (532 nm) laser and a red (633 nm) laser. From the two spectra, one can clearly see that in this sample, the region near the *i/p* interface has lower crystalline volume fraction than the bulk of the intrinsic layer. We deconvoluted the Raman spectra into different components of amorphous LA (~310 cm^{-1}), LO (~380 cm^{-1}), TO (~480 cm^{-1}), intermediate (~500 cm^{-1}), and crystalline (~520 cm^{-1}) modes. Table VI lists the parameters of the amorphous TO, intermediate, and the crystalline modes. It is common to determine the crystalline volume fraction from the area under each deconvoluted curve, with a correction factor for the grain size dependence of Raman cross-section [21,22]. For simplicity, we only present the ratio of areas for each component. To emphasize the key points, Fig. 8 plots (upper panel) initial and stable efficiencies with a comparison to (lower panel) the fractions of each Raman component obtained by deconvolution of the Raman spectra measured using the green and red lasers. From Table VI and Fig. 8, three important phenomena are observed. First, the crystalline volume fraction (the narrow peak at ~520 cm^{-1}) is higher for the green laser than the red laser in the samples with constant hydrogen dilution (Sample 10514), as normally observed in the nanocrystalline evolution with thickness. The optimized hydrogen dilution profiling (Samples 10505 and 13348) reversed this trend and resulted in a lower crystalline volume fraction in the region near the *i/p* interface as previously reported [7]. Second, the stable cells have lower crystalline volume fractions than those with high light-induced degradation, especially at the *i/p* interface region probed by the green light. Third, although the crystalline peak is smaller in the stable cells than in the unstable samples, the intermediate range peak is not smaller. In fact, it becomes broader and shifts to lower wave numbers.

From the three observations, we believe that the light-induced degradation in nc-Si:H solar cells does not necessarily increase (instead, it decreases in our solar cells) with increasing amorphous volume fraction. Also, it appears that the stable cells have a relatively large and broad intermediate Raman peak. It is reasonable to speculate that this intermediate peak plays a role in the metastability. The origin of the intermediate Raman peak could be due to the intermediate range order [23,24], such as

Table VI: Raman deconvolution data for six nc-Si:H solar cells measured with green (532.0 nm) and red (632.8 nm) lasers. a, i, and c denote the three peaks corresponding to the amorphous TO, intermediate, and the crystalline TO peaks. p, w, and f denote the peak position, width, and area percentage of each peak.

Run #	λ (nm)	a			i			c		
		p_a (cm^{-1})	w_a (cm^{-1})	f_a (%)	p_i (cm^{-1})	w_i (cm^{-1})	f_i (%)	p_c (cm^{-1})	w_c (cm^{-1})	f_c (%)
10514	532.0	469.1	78.7	45.1	501.2	37.8	27.3	517.1	10.2	27.6
	632.8	481.6	65.7	59.0	510.7	21.5	16.7	519.1	10.3	24.3
10521	532.0	483.7	65.5	36.5	508.4	27.6	24.7	518.6	10.2	38.9
	632.8	485.4	65.6	46.1	511.6	24.3	21.2	520.9	10.3	32.8
10505	532.0	457.5	70.1	45.2	486.8	53.9	50.9	514.2	13.1	3.9
	632.8	471.3	64.8	57.0	499.4	41.2	26.5	518.1	11.2	16.5
12085	532.0	479.4	69.9	56.5	505.5	29.1	17.1	518.6	11.6	26.4
	632.8	483.5	63.8	49.9	509.7	24.3	19.6	520.0	11.2	30.5
13324	532.0	480.8	67.0	58.0	508.4	26.1	18.4	518.6	8.7	23.5
	632.8	484.4	65.6	47.3	511.6	25.2	23.9	520.9	9.3	28.8
13348	532.0	467.7	68.5	61.8	496.8	43.6	30.4	518.6	10.2	7.7
	632.8	480.7	63.8	60.1	508.8	29.0	19.1	520.0	10.3	20.8

the linear-like structure in high hydrogen diluted a-Si:H, and/or from grain boundaries [22,25]. The observed improved stability of high hydrogen diluted a-Si:H was suggested to be due to the intermediate range order [23,24]. At this time, we believe that both assignments are possible, depending on the structure of the material. In our case, when the nc-Si:H intrinsic layer was deposited under a controlled hydrogen dilution profiling, although a significant amount of small grains was incorporated in the material, they were not allowed to grow into larger grains. These small grains may not contribute to the sharp crystalline Raman peak, but can contribute to the intermediate peak. From the correlation between the solar cell stability results and the Raman analyses, we speculate that our stable nc-Si:H cells have a large amount of small grains and intermediate range order, especially near the *i/p* interface.

The increase of the intermediate orders along the growth direction is also an important feature. It is known that the *i/p* interface is the dominant junction in an *n-i-p* (or *p-i-n*) structure [26]. The small grains with a reasonable amount of amorphous component in the *i/p* interface region may provide a good grain boundary passivation and a compact material structure, which reduce defect density and any impurity diffusion. As a result, the open-circuit voltage (V_{oc}) of the cell is improved. The high crystalline volume fraction in the bulk of the nc-Si:H intrinsic layer, especially in the *n/i* region, ensures sufficient long wavelength absorption resulting in a high short-circuit current density (J_{sc}); it also provides high mobility paths for carrier transport resulting in an improved fill factor (FF). One may suspect that the amorphous component in the *i/p* region would cause extra light-induced degradation. In fact, it is true that the J_{sc} in some hydrogen-dilution profiled nc-Si:H cells, such as #13324 and #13348 in Table V, decreases due to the short wavelength response. The reduced short wavelength response is due to recombination in the amorphous phase near the *i/p* interface and can be annealed back at a high temperature. We also observed a loss of FF measured under blue light (not shown). The FF measured under white light is not significantly affected because the transport of carriers generated in the bulk of the intrinsic layer goes through the nanocrystalline path with well passivated grain boundaries. From this result, we believe that a decrease of crystalline volume fraction and grain size along the growth direction in a nc-Si:H *n-i-p* structure near the *i/p* interface is beneficial for the cell performance and stability. This feature can be obtained by reducing hydrogen dilution during the nc-Si:H deposition in the *n-i-p* structure and can also occur naturally when the nc-Si:H intrinsic layer in a *p-i-n* structure is deposited on the *p* layer [11].

Based on the above results, we have further optimized the deposition conditions, including the hydrogen dilution profile, and achieved an initial active-area efficiency of 8.99% in a nc-Si:H single-junction cell. Using optimized nc-Si:H cells in an a-Si:H/nc-Si:H/nc-Si:H triple-junction structure, we have achieved initial and stable active-area efficiencies of 14.1% and 13.3%, respectively, as presented in the previous section. The J_{sc} in the nc-Si:H middle and bottom cells shows very little change after prolonged light soaking. The overall cell performance degradation is only 6.4% after prolonged light soaking.

2.4. SUMMARY

Three conclusions have been drawn about the metastability of nc-Si:H solar cells. First, the amorphous component is not necessarily the determining factor for the light-induced degradation in nc-Si:H solar cells. Second, smaller grains and intermediate range order may provide a better grain boundary passivation, and hence improve the cell stability. Third, a decrease of crystalline volume fraction along the growth direction in an *n-i-p* structure, especially near the *i/p* interface, can improve the cell performance and the stability. This has been accomplished by an optimized hydrogen dilution profile. Based on the above findings and understanding, we have further improved the nc-Si:H material

quality. By incorporating the improved nc-Si:H material in both the middle and bottom cells of an a-Si:H/nc-Si:H/nc-Si:H triple-junction structure, we have achieved initial and stable active-area efficiencies of 14.1% and 13.2%, respectively, as shown in the previous section.

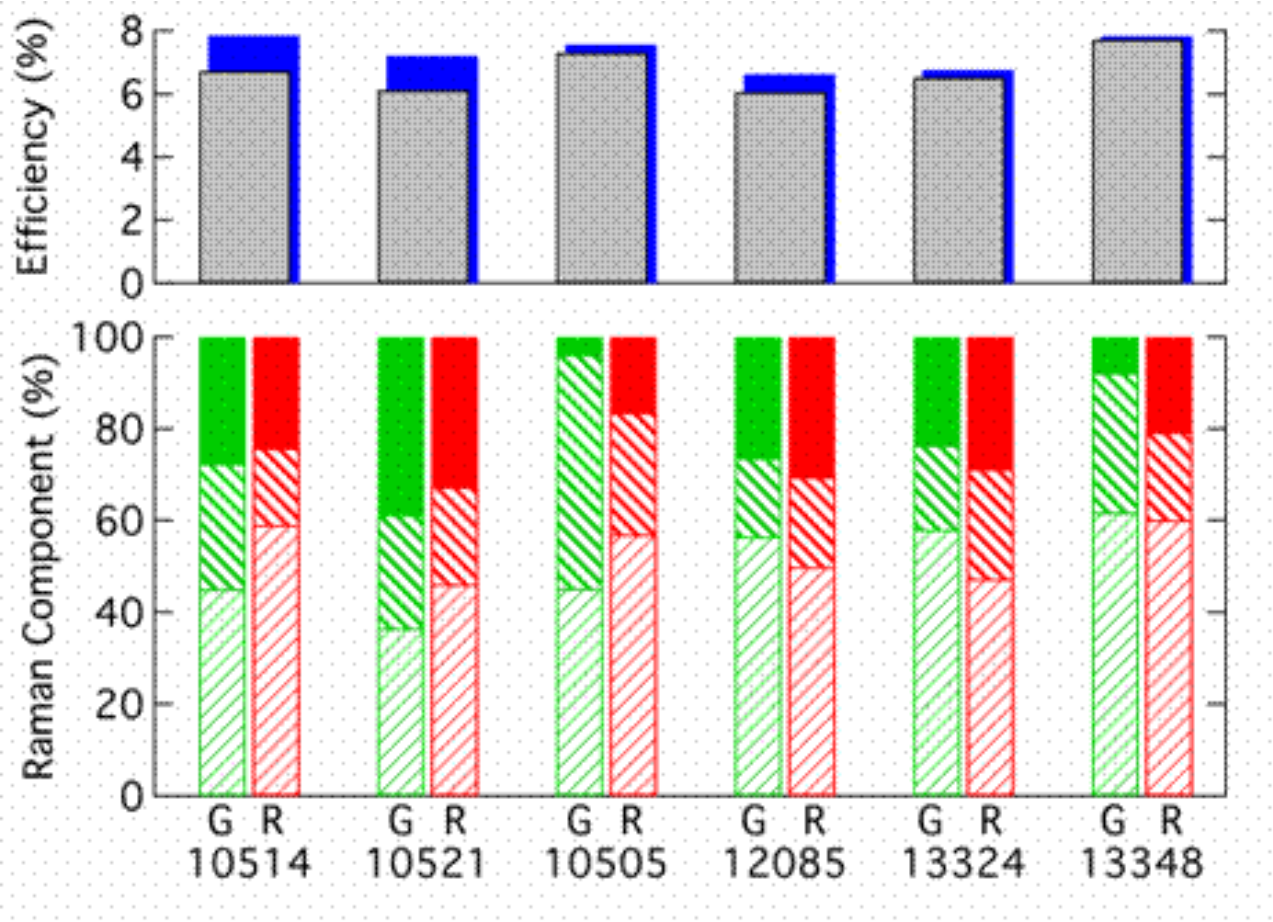

Figure 8. The upper plot shows the initial (back block) and stable (front block) efficiencies of nc-Si:H solar cells. The lower plot shows the fractions of different Raman components of amorphous (lower block), intermediate (middle block), and crystalline (upper block) modes in nc-Si:H cells measured with 532-nm (G) and 633-nm (R) lasers.

REFERENCES

[1] J. Yang, A. Banerjee, and S. Guha, Appl. Phys. Lett. **70**, 2975 (1997).

[2] S. Guha, Mater. Res. Soc. Symp. Proc. **808**, 521 (2004).

[3] K. Yamamoto, *et al*., Technical Digest, 15th International Photovoltaic Science and Engineering Conference, Shanghai, China, October 10-15, 2005, p. 529.

[4] K. Saito, M. Sano, S. Okabe, S. Sugiyama, and K. Ogawa, Sol. Energy Mater. & Solar Cells **86**, 565 (2005).

[5] B. Yan, G. Yue, J. Yang, A. Banerjee, and S. Guha, Mat. Res. Soc. Symp. Proc. **762,** 309 (2003).

[6] B. Yan, G. Yue, J. Yang, K. Lord, A. Banerjee, and S. Guha, Proc. of 3rd World Conference on Photovoltaic Energy Conversion, May 11-18, 2003, Osaka, Japan, p. 2773.

[7] B. Yan, G. Yue, J. Yang, S. Guha, D. L. Williamson, D. Han, and C.-S. Jiang, Appl. Phys. Lett. **85**, 1955 (2004).

[8] B. Yan, J. M. Owens, J. Yang, and S. Guha, Proc. of 31st IEEE Photovoltaic Specialists Conference, Lake Buena Vista, FL, January 3-7, 2005, p. 1456.

[9] G. Yue, B. Yan, G. Ganguly, J. Yang, S. Guha, C. W. Teplin, and D.L. Williamson, Proc. of 4th World Conference on Photovoltaic Energy Conversion, May 7-12, 2006, Hawaii, USA, in press.

[10] L. Guo, M. Kondo, M. Fukawa, K. Saitoh, and A. Matsuda, Jpn. App. Phys. Part 2 **37,** L1116 (1998).

[11] Y. Mai, S. Klein, R. Carius, J. Wolff, A. Lambertz, F. Finger, and X. Geng, J. Appl. Phys. **97,**114913 (2005).

[12] J. Meier, R. Flückiger, H. Keppner, and A. Shah, Appl. Phys. Lett. **65**, 860 (1994).

[13] O. Vetterl, F. Finger, R. Carius, P. Hapke, L. Houben, O. Kluth, A. Lambertz, A. Mück, B. Rech, and H. Wagner, Sol. Energy Mater. Sol. Cells **62**, 97 (2000).

[14] K. Yamamoto, IEEE Trans. on Electron Device **46**, 2041 (1999).

[15] B. Yan, G. Yue, J. M. Owens, J. Yang, and S. Guha, Appl. Phys. Lett. **85**, 1925 (2004).

[16] G. Yue, B. Yan, J. Yang, and S. Guha, Appl. Phys. Lett. **86**, 092103 (2005).

[17] G. Yue, B. Yan, J. Yang, and S. Guha, J. Appl. Phys. **98**, 074902 (2005).

[18] S. Klein, F. Finger, R. Carius, T. Dylla, B. Rech, M. Grimm, L. Houben, and M. Stutzmann, Thin Solid Films **430**, 202 (2003).

[19] F. Meillaud, E. Vallat-Sauvain, X. Niquille, M. Dubey, J. Bailat, A. Shah, and C. Ballif, Proceeding of the 31st IEEE Photovoltaic Specialists Conference, Florida, USA, January 3-7, 2005, p. 1412.

[20] T. Roschek, T. Repmann, J. Müller, B. Rech, H. Wagner, Proceeding of 28th IEEE Photovoltaic Specialists Conference, Anchorage, AK, September 15-22, 2000, p. 150.

[21] E. Bustarret, M. A. Hachicha, and M. Brunel, Appl. Phys. Lett. **52**, 1675 (1988).

[22] D. Han, J. D. Lorentzen, J. Wenberg-Wolf, L. McNeil, and Q. Wang, J. Appl. Phys. **94**, 2930 (2003).

[23] D. V. Tsu, B. S. Chao, S. R. Ovshinsky, S. Guha, and J. Yang, Appl. Phys. Lett. **71**, 1317 (1997).

[24] D. V. Tsu, B. S. Chao, S. R. Ovshinsky, S. J. Jones, J. Yang, S. Guha, and R. Tsu, Phys. Rev. B **63**, 125338 (2001).

[25] S. Veprek, F.-A. Sarott, and Z. Iqbal, Phys. Rev. B **36**, 3344 (1987).

[26] A. Pawlikiewicz and S. Guha, Mat. Res. Soc. Symp. Proc. **118**, 599 (1988).